HHS Public Access

Author manuscript

Nat Med. Author manuscript; available in PMC 2018 October 16.

Published in final edited form as:

Nat Med. 2018 May ; 24(5): 617–627. doi:10.1038/s41591-018-0003-0.

Differential Glucose Requirement in Skin Homeostasis and Injury Identifies a Therapeutic Target for Psoriasis

Zhuzhen Zhang[1], **Zhenzhen Zi**[*,2], **Eunice E. Lee**[*,1], **Jiawei Zhao**[1], **Diana C. Contreras**[3], **Andrew P. South**[4], **E. Dale Abel**[5], **Benjamin F. Chong**[1], **Travis Vandergriff**[1], **Gregory A. Hosler**[1,6], **Philipp E. Scherer**[7,8], **Marcel Mettlen**[8], **Jeffrey C. Rathmell**[3], **Ralph J. DeBerardinis**[9,10,11], and **Richard C. Wang**[1]

[1]Department of Dermatology, UT Southwestern Medical Center, Dallas, TX, 75390

[2]Department of Biochemistry, UT Southwestern Medical Center, Dallas, TX, 75390

[3]Department of Pathology, Microbiology, and Immunology, Vanderbilt University Medical Center, Nashville, Tennessee, USA.

[4]Department of Dermatology & Cutaneous Biology, Thomas Jefferson University, Philadelphia, PA, 19107

[5]Fraternal Order of Eagles Diabetes Research Center and Division of Endocrinology and Metabolism, Roy J. and Lucille A. Carver College of Medicine, University of Iowa, Iowa City, IA, 52242

[6]ProPath, Dallas, TX, 75247

[7]Touchstone Diabetes Center, Department of Internal Medicine, UT Southwestern Medical Center, Dallas, TX, 75390, Dallas, Texas, USA

[8]Department of Cell Biology, UT Southwestern Medical Center, Dallas, TX, 75390

[9]Children's Medical Center Research Institute, UT Southwestern Medical Center, Dallas, 75390

[10]Department of Pediatrics, UT Southwestern Medical Center, Dallas, TX, 75390

[11]Eugene McDermott Center for Human Growth and Development, UT Southwestern Medical Center, Dallas, TX, 75390

Abstract

Corresponding author: Richard C. Wang, MD PhD, Office: 214-648-3430, richard.wang@utsouthwestern.edu.
*These authors contributed equally

Contributions

Z.Zh., R.J.D., and R.C.W. designed the experiments. Z.Zh., E.E.L., J.Z., M.M., and R.C.W. performed experiments. E.D.A. provided *Glut1*$^{fl/fl}$ mice. A.P.S. provided SCCT8 squamous cell carcinoma cells. B.F.C. enrolled control and psoriasis patients. Z.Zh., Z.Zi, E.E.L., J.Z., D.C.C., M.M., G.A.H., T.V., J.C.R., P.E.S., R.J.D., and R.C.W. analyzed data; R.C.W. and Z.Zh. wrote the manuscript with contributions from all authors.

Competing interests

The authors declare no competing financial interests.

Proliferating cells depend on glucose uptake more than quiescent cells for their growth. While glucose transport in keratinocytes is mediated largely by the *Glut1* facilitative transporter, the keratinocyte-specific ablation of *Glut1* did not compromise mouse skin development and homeostasis. *Ex vivo* metabolic profiling revealed altered sphingolipid, hexose, amino acid, and nucleotide metabolism in *Glut1*-deficient keratinocytes, suggesting metabolic adaptation. On the other hand, *Glut1*-deficient keratinocytes in culture displayed metabolic and oxidative stress and impaired proliferation. Similarly, *Glut1* deficiency impaired *in vivo* keratinocyte proliferation and migration within wounded or UV-damaged mouse skin. Notably, both genetic and pharmacological *Glut1* inactivation reduced hyperplasia in mouse models of psoriasis-like disease. Topical application of a Glut1 inhibitor also reduced inflammation in these models. Glut1 inhibition decreased expression of pathology-associated genes in human psoriatic skin organoids. Thus, Glut1 is selectively required for injury- and inflammation-associated keratinocyte proliferation, and its inhibition offers a novel treatment strategy for psoriasis.

Keywords

Glut-1; glucose metabolism; keratinocyte; psoriasis; wound healing; UV irradiation

INTRODUCTION

Glucose is a preferred bioenergetic and synthetic substrate for rapidly proliferating cells. However, recent studies have begun to highlight the diverse array of metabolic substrates that cells can use to promote growth. For example, although cancer cells consistently show a high capacity to utilize glucose as a metabolic substrate[1], they are capable of using diverse substrates (e.g. amino acids, acetate, lactate) for energy generation and anabolic growth *in vivo*[2–6]. In some tissues, the preferential utilization of glycolysis has been linked to a cell's phenotype. For example, increased Glut1 expression and glucose utilization promote effector T cell function while fatty acid oxidation promotes regulatory CD4+ T cell and memory CD8+ T cell fates[7,8]. In endothelial cells, glycolysis promotes vessel branching and migration while fatty acid oxidation is required for proliferation[9,10]. Thus, tissue functions are regulated in part through the controlled flow of metabolic substrates.

The facilitative glucose transporters (Glut's) regulate the availability of glucose for most tissues. The thirteen GLUT family members are regulated in a tissue- and stimulus- specific fashion, suggesting important roles in shaping or maintaining cell function[11]. Glut1 is the most widely expressed facilitative glucose transporter and regulates basal glucose uptake in most tissues[12], including the basal cells of the epidermis[13]. Consistent with a role in promoting keratinocyte proliferation, Glut1 expression is increased in wound healing, in psoriatic plaques, or after UV-induced hyperplasia[14–16]. However, the precise role for Glut1 and glucose transport in regulating keratinocyte function has not been definitively characterized.

Here, we specifically deleted *Glut1* in keratinocytes to determine how glucose metabolism affects epidermal development and function. Consistent with its known role in energy generation and biosynthesis, *Glut1* deficient keratinocytes show markedly impaired

proliferation *in vitro*. Yet, *Glut1* deficiency had no impact on epidermal development or function *in vivo*. Gene expression analyses, metabolic profiling, and *in vitro* rescue experiments revealed that alternative hexoses, amino acid catabolism, and fatty acid oxidation could all contribute to metabolic programs that allowed for epidermal function in the absence of *Glut1*. However, *Glut1* deficiency impaired the physiological proliferation triggered by full-thickness wounds and UV irradiation, and genetic or chemical inhibition of Glut1 rendered the skin resistant to imiquimod or IL-23 induced psoriasiform hyperplasia. Thus, glucose metabolism is selectively essential for proliferating keratinocytes highlighting a potential therapeutic target for pathological hyperproliferation.

RESULTS

Glut1 Is Required for Glucose Uptake and Proliferation

Although the expression of *Glut1* in keratinocytes is well established, the regulation of *Glut1* and expression of additional glucose transporters in the skin has not been explored. Immunofluorescence revealed that Glut1 was primarily expressed in the more proliferative basal layers of both human and mouse skin (Fig. S1a). Consistent with the reported role of Glut1 in cell proliferation, the expression of *Glut1* was high in undifferentiated keratinocytes but decreased following either Ca^{2+} or confluence induced differentiation (Fig. S1b, c). The expression of other facilitative (*Glut1-13*) and sodium dependent glucose transporters (*SGLT1-2*) in mouse epidermis, mouse and human primary keratinocytes, immortalized human keratinocytes (HEK001), and squamous cell cancers were assessed[17]; only Glut1 was highly expressed (Fig. S1d–h). Next, *Glut1* was deleted in epidermal keratinocytes by crossing $Glut1^{fl/fl}$ mice to K14-Cre expressing mice (hereafter *K14.Glut1*)[18]. In these mice, *Glut1* mRNA expression was reduced by >95% in both the epidermis and primary cultured keratinocytes compared to their $Glut1^{fl/fl}$ (hereafter *WT*) littermates. Western Blot and immunofluorescence confirmed that Glut1 could not be detected in the epidermis of *K14.Glut1* mice (Fig. 1a, b, S1i–j). Quantitative RT-PCR revealed no significant compensatory upregulation of any other glucose transporters in keratinocytes from *K14.Glut1* mice (Fig. 1c). [^{3}H] 2-deoxyglucose (2-DG) uptake assays in primary *Glut1* deficient keratinocytes confirmed that *Glut1* deletion blocked glucose transport. 2-DG uptake was decreased by ~96% in keratinocytes from *K14.Glut1* versus *WT* littermates. The residual low level of glucose uptake in keratinocytes from *K14.Glut1* mice was comparable to passive levels of transport, which occurred in the presence of chemical inhibitors of glucose transport (Fig. 1d).

Because Glut1 plays important roles in cell proliferation[19,20], we tested whether keratinocytes from *K14.Glut1* mice showed defects in proliferation. The growth of primary *Glut1* deficient keratinocytes was markedly impaired compared *WT* keratinocytes as assessed by Crystal Violet staining and cell number (Fig. 1e). GLUT1 was also essential for proliferation in human keratinocytes *in vitro*. The chemical inhibition of glucose transport through an established inhibitor of glucose transport, WZB117[21], impaired glucose uptake and significantly slowed cell growth compared to vehicle control (Fig. S2a–b). Consistent with the 2-DG uptake studies, keratinocytes from *K14.Glut1* mice consumed less glucose and produced less lactate (~5%) than their *WT* counterparts (Fig. 1f). ATP levels were also

significantly lower in these keratinocytes (Fig. 1g). Decreased ATP levels can cause energetic stress and activate the 5' AMP-activated protein kinase (AMPK). Indeed, downstream targets of AMPK like acetyl-CoA carboxylase 1 (ACC) showed increased phosphorylation in the knockout keratinocytes. Consistent with this energetic stress, phosphorylation of S6 ribosomal protein, a target of the mTOR and a growth-promoting pathway, was inhibited in keratinocytes from *K14.Glut1* mice compared to *WT* controls (Fig. 1h).

Glut1 Contributes to Redox Homeostasis

To discover additional pathways contributing to the impaired proliferation in glucose deficiency, we performed microarray analysis on keratinocytes from *K14.Glut1* mice and their *WT* littermates (GSE102955, Fig. 2a, S3a). Consistent with the significantly decreased proliferative capacity of *Glut1* deficient keratinocytes, hierarchical clustering and gene ontology analyses revealed that genes related to the cell cycle progression and cell division were markedly impaired compared to keratinocytes from their *WT* littermates. Normal cells respond to oxidative stress by routing glucose through the pentose phosphate pathways (PPP) to regenerate NADPH[22,23]. Consistent with glucose's role in ROS clearance, transcripts related to redox homeostasis were amongst the most markedly elevated genes in keratinocytes from *K14.Glut1* mice compared *WT* animals (Fig. 2a, S3a). Twenty-four genes related to oxidative stress were more than 2 fold higher in *Glut1* deficient keratinocytes compared to *WT* keratinocytes (Fig. 2b, S3b). Other oxidative stress response genes including *Nqo1* and *Hmox1* (HO1) were significantly upregulated in Glut1 deficient keratinocytes both under basal growth conditions and when cells were treated with H_2O_2 or UVB compared to *WT* keratinocytes (Fig. 2c, d). Confirming the impact of Glut1 on cellular levels of oxidative stress, measurements of DCFDA fluorescence revealed that keratinocytes from *K14.Glut1* mice showed significantly higher levels of reactive oxygen species both under basal growth conditions and after treatment with H_2O_2 or UVB compared to *WT* keratinocytes (Fig. 2e). *Glut1* deficient keratinocytes were significantly more sensitive to H_2O_2 and UVB induced cell death than *WT* keratinocytes even when controlling for their slower growth (Fig. 2f). The supplementation of antioxidants (GSH and NAC) rescued H_2O_2-induced toxicity in keratinocytes from *K14.Glut1* mice (Fig. 2g). In primary human keratinocytes, the acute inhibition of GLUT1 through WZB117 also increased the sensitivity of the cells to H_2O_2 (Fig. S2c) and increased the expression of redox homeostasis genes (Fig. S2d). Both genetic and chemical inhibition of glucose transport lowered levels of NADPH compared to their respective controls (Fig. 2h, S2e–f), suggesting that decreased flux through the PPP contributed to the observed defects in redox homeostasis. MitoSOX staining further revealed that the acute (but not chronic) chemical inhibition of glucose transport increased mitochondrial oxidative stress compared to vehicle control (Fig. S2g), suggesting mitochondria as an additional source of oxidative stress in keratinocytes deprived of glucose. Despite Nrf2's established role in mediating the response to oxidative stress[24], total and nuclear levels of Nrf2 were not higher in keratinocytes from *K14.Glut1* mice (Fig. S4a–b). Thus, Glut1 is required for redox homeostasis in keratinocytes at least in part through its roles in regenerating NADPH.

Glut1 Is Not Essential for Normal Skin Development

Given the striking impact of *Glut1* deletion on the keratinocyte growth, we assessed the *in vivo* impact of *Glut1* deletion. Notably, *K14.Glut1* mice were overtly normal. We observed no abnormalities in the skin of young or adult *K14.Glut1* mice relative to their *WT* littermates (Fig. S5a). Both male and female *K14.Glut1* mice demonstrated normal skin histology at one week and 2 months (Fig. 3a). The expression and localization of epidermal keratins (K10 and K14) (Fig. 3b, S5b–d), loricrin (Fig. S5e), and differentiation and adhesion genes (Fig. 3c) showed no differences between *WT* and *K14.Glut1* littermates, suggesting that epidermal differentiation was normal.

Given previous reports that glycosylated ceramides and UDP-glucose are essential intermediates for epidermal ceramide maturation, lamellar body formation, and stratum corneum development[25,26], we performed an analysis of epidermal lipids. LC-MS/MS revealed that the epidermis of *K14.Glut1* mice showed unchanged levels of phospholipids, lower levels of free ceramides and sphingoidbases, and higher levels of sphingomyelins (Fig. 3d, S5f, Lipidomics Data Set). Notably, while hexosylceramide levels were significantly decreased in keratinocytes from *K14.Glut1* mice, they were not significantly decreased in the epidermis of *K14.Glut1* neonatal mice compared to *WT* (Fig. 3e). Moreover, *K14.Glut1* mice showed no significant differences in weight from *WT* littermates either as pups or adults (Fig. 3f). Compared to *WT* embryos, *K14.Glut1* embryos showed both a normal toluidine blue exclusion assay (Fig. 3g) and no defects in transepidermal water loss as assessed by a weight time-course analysis of newborn mice (Fig. 3h). Finally, in contrast to the previously described defects in redox homeostasis, *Glut1*-deficient epidermis showed no marked alterations in the expression of redox homeostasis genes or evidence of energetic stress by Western blot analyses (Fig. S5g–h). Thus, while keratinocytes from *K14.Glut1 mice* showed marked alterations in lipid metabolism, redox homeostasis, and energetic stress *in vitro*, these defects are rescued *in vivo* allowing the normal skin development.

Metabolic Compensation for Glut1 Deficiency

To gain insight on how *K14.Glut1* mice adapted to the loss of glucose uptake, neonatal epidermis was harvested for the analysis of intracellular metabolites by LC-MS/MS (Metabolomics Data Set). Principal component analysis showed different metabolic profiles for epidermis from *K14.Glut1* versus *WT* mice (Fig. S6a). Quantitative pathway enrichment analysis of epidermal metabolites from Glut1 deficient mice compared to littermate controls revealed the significant enrichment of several expected pathways including nucleotide sugar metabolism, the tricarboxylic acid (TCA) cycle, and the pentose phosphate pathway (Fig. S6b). Significantly lower levels of numerous metabolites, including Glucose-6P, lactate, aconitate, malate, and fumarate, confirmed the expected impairments in glycolysis and the TCA cycle (Fig. 4a). Metabolomics also revealed significant changes in amino acid metabolism and the urea cycle including changes in glutamine, cystathionine, citrulline, carbamoyl phosphate and acetylornithine (Fig. 4b). Consistent with the increased catabolism of amino acids, the expression of numerous amino acid transporters were significantly higher in keratinocytes from *K14.Glut1* mice compared to *WT* controls (Fig. S6c). Finally, *Glut1* deletion also impacted nucleotide metabolism as evidenced by lower levels of uridine

monophosphate (UMP) and dAMP and higher allantoin in epidermis from *K14.Glut1* compared to *WT* controls (Fig. 4c).

Metabolic profiling highlighted changes in galactose metabolism in the epidermis of *K14.Glut1* mice. Intracellular galactose-1P is maintained at similar levels as glucose-6P/fructose-6P (G6P/F6P) and is depleted to similar levels as G6P/F6P in the epidermis of *K14.Glut1* mice suggesting that it was actively metabolized in the epidermis (Fig. 4a). Moreover, keratinocytes express *Glut5, SGLT1* (Fig. S1d–e), and ketohexokinase which should allow for fructose metabolism to occur. Therefore, we tested whether galactose and fructose could rescue the growth of *Glut1* deficient keratinocytes. Both fructose and galactose significantly improved the growth of *Glut1* deficient keratinocytes (Fig. 4e–f; S7a,b), ATP levels (Fig. 4g), the expression of redox homeostasis genes (Fig. 4h), and resistance to H_2O_2 (Fig. 4i) compared to keratinocytes from *WT* mice. Fructose almost fully rescued the growth and oxidative stress defects of keratinocytes from *K14.Glut1* mice while galactose was less effective. Because fatty acid oxidation (FAO) contributes reducing equivalents and acetyl-CoA in endothelial cell metabolism[10], we tested whether mixtures of oleate and palmitate could rescue the growth of *Glut1* deficient keratinocytes. Adding up to 10μM of a fatty acid mixture partially rescued the growth of keratinocytes from *K14.Glut1* mice and increased ATP production in both *Glut1* deficient and *WT* keratinocytes (Fig. 4j–k). In contrast, a myriad of downstream metabolites and antioxidants including pyruvate, lactate, amino acids, GSH, NAC, glutamine, or ribose supplemented individually or in combinations (Fig. S7c–h) and growth under hypoxic conditions (Fig. S7i) were unable to rescue *Glut1* deficient keratinocyte growth *in vitro*. In summary, keratinocytes can utilize galactose, fructose, and fatty acids as metabolic substrates to promote growth in the absence of *Glut1* (Fig. S7j).

Glut1 Is Required for Stress Responses *In vivo*

We next tested whether Glut1 was necessary for the epidermal responses to physiological stress. One critical function of human skin is protection from UV irradiation. Chronic irradiation has been reported to promote both *Glut1* expression and acanthosis[16]. We shaved and Ultraviolet B irradiated (UVB) *K14.Glut1* mice and *WT* littermates to determine the role of glucose transport in the acute and delayed response to UVB (Fig. S8a). There were no obvious macroscopic or histologic differences between the skin of *K14.Glut1* mice and *WT* littermates 24 hours after UVB (Fig. 5a, S8a–b). UVB induced similar, significant increases in skin thickness for both *WT* and *K14.Glut1* mice (Fig. S8c). TUNEL staining for apoptotic keratinocytes also showed no differences between the skin of *WT* and *K14.Glut1* mice (Fig. S8d–e). Five days after UVB, *WT* mice had largely recovered and showed regular acanthosis while many areas of skin from *K14.Glut1* mice showed areas of abnormal stratification with areas of keratinocyte necrosis (Fig. 5a, S8b). While non-irradiated epidermis did not show differences in redox homeostasis genes, 6 hours after UVB, *Glut1* deficient epidermis showed a modest, but significant, upregulation of oxidative stress response genes compared to epidermis from *WT* controls. These changes were no longer significant 24 hours after UVB (Fig. 5b, S5g, S8f). Significantly fewer Ki-67+ cells were present in the epidermis of *K14.Glut1* mice than *WT* controls (Fig. 5c,d). These defects in proliferation were corroborated by elevated staining of p-ACC Ser79 and decreased staining

of p-S6 Ser240/244 in the skin of *Glut1* deficient mice compared to *WT* controls after UVB (Fig. S8e). Keratinocytes secrete inflammatory cytokines in response to UVB[27], which contributes to the physiological response to irradiation. UVB-induced inflammation, as assessed by the expression of *IL1β, TNFα, IL6, IFNγ*, revealed no significant differences between littermates (Fig. S8g). In summary, compared to *WT* mice, *K14.Glut1* mice show impairments in redox homeostasis, proliferation, and recovery after UVB..

The epidermis also undergoes rapid proliferation in response to wounds. To understand the role of Glut1 in wound repair, we assessed the recovery of mice from splinted 3-mm excisional wounds (Fig. S9a). Re-epithelialization was assessed after 5.5 and 8 days. Both *K14.Glut1* and *WT* mice exhibited lymphohistiocytic infiltrates around the wound edge (Fig. S9b). However, healing in the *K14.Glut1* mice was significantly impaired at both time points compared to *WT* littermates (Fig. 5e–f). Specifically, *WT* mice had largely completed wound healing by day 8 while all *K14.Glut1* mice still exhibited persistent epidermal defects (Fig. 5e, S9b). Keratinocyte migration and proliferation both contribute to wound healing.[28] To study cell migration in *Glut1* deficient keratinocytes, we analyzed keratinocytes migration after a scratch assay by time-lapse microscopy. Keratinocytes from *K14.Glut1* mice showed significantly delayed scratch closure compared to cells from *WT* littermates (Fig. 5g–h, Movie S1–2). To address the role of proliferation in re-epithelialization, we assessed the histology of wound edge. Wounds in *K14.Glut1* had significantly fewer Ki-67 positive cells within 500μm of the wound edge than *WT* controls (Fig. S9c). Consistent with these *in vitro* proliferative defects, the excisional wounds of *K14.Glut1* mice also showed elevated staining of p-ACC Ser79 and decreased staining of p-S6 Ser240/244 (Fig. S9e).

Glucose Transport Inhibition Ameliorates Psoriasis Models

Although keratinocyte hyperproliferation can be triggered as a protective response against physiological insults, it can also be triggered pathologically. Psoriasis is a chronic cytokine-driven, inflammatory skin disease characterized by hyperplasia and abnormal differentiation of the epidermis that presents as thickened and scaly plaques. After confirming that *GLUT1* transcription and expression were elevated in lesional biopsies from psoriasis patients (Fig. S10a–c), we tested whether Glut1 deletion might impact the development of pathological hyperplasia in diseases like psoriasis. We established psoriasiform hyperplasia in *WT* and *K14.Glut1* mice through two models—topical application of imiquimod[29,30] and intradermal injection of IL-23[31]. The skin of *WT* mice treated with imiquimod upregulated *Glut1* expression (Fig. S10a, d, e) and showed acanthosis (Fig. S10a). In contrast, the epidermis of *K14.Glut1* mice were markedly protected from imiquimod-induced psoriasiform hyperplasia (Fig. 6a, S10g). To extend the translational relevance of these findings, we tested whether the topical inhibition of glucose transport might also prevent the development of psoriasiform hyperplasia (Fig. S10f). In both mouse models of psoriasiform hyperplasia, treatment with a topical GLUT inhibitor, WZB117, decreased scale (Fig. 6a, S10g–h) and significantly inhibited skin thickening (Fig. 6b–c, S10h) compared to vehical treated mice. The skin of *K14.Glut1* mice and WZB117 treated *WT* mice both showed decreased Ki-67 staining compared to vehicle treated *WT* controls (Fig. 6d–e). Western blots confirmed that both the skin of *Glut1* deficient mice and WZB117 treated mice showed higher p-ACC and decreased p-S6 S240/S244 consistent with energetic stress (Fig. S10i).

In addition to keratinocyte proliferation, imiquimod also induces the accumulation of leukocytes in the skin, including neutrophils, macrophages, dendritic cells, and T cells[30,32,33]. We examined the effect of inhibiting glucose transport on inflammation through immunohistochemical staining. Topically applied WZB117 significantly reduced the number of leukocytes (CD45+), neutrophils (Gr-1+), macrophages (F4/80+), and T cells (CD4+), but not dendritic cells (CD11c) localized to the skin after imiquimod treatment compared to vehicle control. In contrast, the skin of *K14.Glut1* mice only showed significant decreases in T cell number (CD4+) after imiquimod treatment (Fig. 6f, S11a–f). Similarly, several cytokines (*Ccl3, Cxcl3, IL1b*), which are induced in imiquimod induced psoriasiform dermatitis[34], showed significant decreases after topical treatment with WZB117, but not in the *K14.Glut1* mice, compared to vehicle control treated *WT* mice (Fig. S10j). Finally, we applied WZB117 topically to human psoriatic skin organoids[35], WZB117 inhibited the expression of several psoriatic biomarkers (*CXCL3, Elafin, HBD-2, S100A7,* and *S100A8*) in a dose dependent fashion (Fig. 6g). Thus, while genetic *Glut1* deletion rescued only the epidermal acanthosis and proliferation, the topical, chemical inhibition of glucose transport rescued both keratinocyte proliferation and prevented inflammation in animal and organoid models of psoriasiform inflammation.

DISCUSSION

The epidermis is a self-renewing organ that protects the body against environmental insults and excess water loss[36]. How glucose uptake and metabolism contribute to these essential processes has not been explored *in vivo*. Through the deletion of the *Glut1* transporter in keratinocytes, we find that glucose uptake is critical for rapid keratinocyte proliferation and an efficient response to physiologically relevant stressors including full-thickness wounds and UVB irradiation. Despite evidence of stressed energy metabolism and oxidative stress *in vitro, K14.Glut1* mice show normal epidermal development. In contrast to many other tissues, Glut1 is the only significant hexose transporter expressed in keratinocytes, and its deletion largely abolished glucose transport. Thus, our metabolic analyses of Glut1 deficient keratinocytes have broader implications on how other tissues and cancer cells might adapt to a general block of glucose metabolism.

Because glucose contributes to several metabolic pathways, cells induced multiple compensatory pathways in its absence. Our findings highlight the importance of the PPP in the skin, which had previously been demonstrated *in vitro*[22,37]. Transcriptional upregulation of many oxidative stress response genes was noted in the *Glut1* deficient keratinocytes. In the face of decreased hexose availability, metabolic processes involving central carbon metabolism including glycolysis, the TCA cycle, and nucleotide synthesis were suppressed. Transcriptional and metabolomic analyses suggested that alterations in amino acid metabolism might help to maintain these biosynthetic cycles. Specifically, the pattern of alterations in amino acid metabolism could be explained by an increased catabolism of specific amino acids to generate ketoacids (e.g. α-ketoglutarate from glutamine and α–ketobutyrate form cystathionine) to compensate for the loss of glucose. In addition to alterations in amino acid metabolism, we also found that fatty acids could also partially rescue proliferative defects in *Glut1* deficient keratinocytes. *In vitro*, alternative hexoses, especially fructose, could rescue the proliferative defects of *Glut1* deficiency. Despite the

low circulating levels of these hexoses[38,39], galactose was detected intracellularly in both normal and *Glut1* defecient epidermis, suggesting that these hexoses could contribute to normal skin development in the absence of glucose. Galactose rescued growth less efficiently than fructose, reflecting either the inefficient transport of galactose by non-Glut1 facilitative glucose transporters or limitations in the efficiency of the Leloir pathway in keratinocytes[40,41]. However, the supplementation of other downstream metabolites did not rescue the growth of keratinocytes from *K14.Glut1* mice. We speculate that the inherent limitations of *in vitro* culture systems[42] and the central role of glucose in diverse metabolic and signaling pathways limited our ability to rescue the growth of *Glut1* deficient keratinocytes.

While the generation of mitochondria-derived ROS are necessary for skin differentiation[43], the increased amounts of oxidative stress caused by loss of glucose transport does not impact skin differentiation. The glycosylation of both proteins and lipids plays an important biochemical role in the skin. Specifically, glycosylated ceramides have been found to be essential for the proper formation of an intact stratum corneum, as the deletion of glucosylceramide synthase (*Ugcg*) results in a disruption of normal ceramide metabolism, aberrant stratum corneum development, and perinatal lethality[26]. Despite defects in hexosylceramide synthesis *in vitro*, we found the skin barrier to be intact suggesting that the epidermis is able to maintain sufficient levels of ceramides for the maturation of epidermal ceramides even in the absence of *Glut1*.

Because glucose uptake is required for proliferating keratinocytes but not for normal skin development and function, our studies suggest that inhibiting glucose transport represents a promising therapy for skin diseases. Antimetabolites that target the heightened biosynthetic requirements of proliferating cells—including methotrexate[44], 5-fluorouracil[45], and mycophenolic acid[46]—are some of the most effective treatments for inflammatory and neoplastic diseases. While most antimetabolite therapies were discovered fortuitously, our analysis of Glut1 has uncovered glucose transport as a potential target. Psoriasis is characterized by excessive, cytokine-driven epidermal hyperplasia[47]. Psoriatic lesions have heightened requirements for glucose uptake and metabolism as evidence by increased *Glut1* expression and PET scans[48]. Metabolomic studies have demonstrated increased levels of some amino acids in the serum patients with psoriasis[49,50]. Our metabolomic analysis of the epidermis of *Glut1* deficient mice revealed decreases in a similar set of amino acids. Levels of sphingoid bases were increased in the serum and skin of patients consistent with our finding that these lipids were decreased in the skin of *Glut1* deficient mice[51]. Comparing the metabolomics from patients to those of Glut1 deficient mice suggested that inhibiting glucose transport could impact metabolic pathways critical to the development of psoriasis. Consistent with this prediction, Glut1 deficient mice were protected from imiquimod-induced psoriasiform hyperplasia. While the systemic administration of a glucose transport inhibitor are predicted to cause neurologic sequelae, hyperglycemia, and lipodystrophy[21,52], these toxicities could be avoided through the topical use of glucose transport inhibitors. Indeed, the topical application of a Glut1 inhibitor was also effective in protecting mice from imiquimod-induced psoriasiform hyperplasia. Similar to the deletion of *Glut1* in keratinocytes, chemical inhibition of Glut1 inhibited the epidermal proliferation and acanthosis. Topical transport inhibitors had the added feature of suppressing the

inflammatory infiltrates and cytokine secretion in animal models of psoriasis and human psoriatic skin organoids, respectively. Consistent with previously reported roles for *Glut1* and glucose metabolism in T lymphocyte activation[20,53], we speculate that the topical application of WZB117 might also inhibit glucose uptake in other cell types in the skin, including infiltrating lymphocytes, and thereby limit inflammation *in vivo*. In summary, our study provides insight into the metabolic reprogramming that allows cells to survive in the absence of glucose metabolism, highlights the role of glucose transport after physiological stressors, and identifies glucose transport as a viable target in hyperproliferative skin diseases.

Online Methods

All animal procedures were performed under protocols approved by the University of Texas Southwestern Medical Center Institutional Animal Care and Use Committee (IACUC). Animal Protocol Number: 2015-101166. All efforts were made to follow the Replacement, Refinement and Reduction guidelines. To minimize discomfort, mice were anesthetized with Ketamine/Xylazine cocktail before being killed. Patients recruited from University of Texas Southwestern Medical Center outpatient clinics provided written informed consent to participate in a research study, which was approved by the UTSW institutional review board. IRB Protocol Number: STU 082010-241.

Animal Models

Glut1fl/fl mice were obtained from Dr. E. Dale Abel[18], K14 driven Cre-recombinase mice were obtained from Jackson Laboratory, and all of them were maintained on the C57BL/6J background. We generated mice lacking Glut1 specifically in epidermal keratinocytes K14.Glut1 by crossing female Glut1$^{fl/fl}$ mice with male K14-Cre mice. Pilot experiments confirmed that previously reported sample sizes for UVB irradiation[54], excisional wound splinting[55], and imiquimod-induced psoriasiform hyperplasia[32] studies would have sufficient power. For UVB lamp irradiation, we first anesthetized the mice with a Ketamine/Xylazine cocktail (Ketamine 120 mg/kg + Xylazine 16 mg/kg), shaved the dorsal hair of 2-month-old female mice, applied a thin layer of Nair on the shaved area for 50–60 seconds, and then washed off the Nair with wet cotton swabs. The dose of UVB lamp was measured by a IL700 Research Radiometer (International Light Technology). Cells or mice were placed at least 20 cm from the light source. For the excisional would splinting model, 2-month-old mice were shave and chemically depilated. The dorsal skin of the mouse, midline between the shoulder and neck of mice, was excised with a 3 mm biopsy punch (Miltex) to the level of the panniculus carnosus. A sterile, circular silicone splint was attached to the skin with Krazy glue, and then secured with 5-0 Prolene sutures. A topical antibiotic (Bacitracin + Polymyxin B + Neomycin) ointment was applied and wounds were dressed with Tegaderm transparent dressing daily. The size of wound was measured at indicated time points. For the imiquimod-induced psoriasiform hyperplasia model, 2-month-old mice were shaved and chemically depilated. The shaved dorsal skin samples were treated topically with 50 mg of Aldara cream (5% Imiquimod) (Aldara, 3M Pharmaceuticals) daily. For the intradermal IL-23 induced psoriasiform hyperplasia model, shaved and depilated 2-month-old mice were injected daily on a labeled location on the central back with 1μg rmIL-23 (ThermoFisher) in

PBS/0.1% BSA. The appearance of the back skin were monitored daily and tissues were harvested, typically after 5 days of treatment. The appearance of the back skin were monitored daily and tissues were harvested, typically after 5 days of treatment. For WZB117 treatment, WT mice were randomly assigned to receive either WZB117 (100μl of 1mg/ml) or the acetone vehicle control. The WZB treatment was applied topically immediately prior to imiquimod treatment or IL-23 injection.

Keratinocyte Culture and Treatments

HEK001 (ATCC CRL-2404) and SCCT8 (obtained from Andrew South) were cultured according to instructions. Human and mouse primary keratinocytes were isolated by dispase digestion[56]. Before digestion, the subcutaneous fat was first removed from human skin. Abdominal human skin excisions or one-week-old mouse skin were floated on 1 U/ml dispase (Invitrogen, 17105-041) in HBSS (Gibco, 14170) for 18 hours at 4°C with dermis side down. The next day, the skin was placed in a new dish with the epidermis side down and the epidermis was peeled and placed into a new dish with HBSS. After washing, the cells were collected into a new 15 mL tube. The epidermis to cut into small pieces, resuspended in HBSS, gently pipetted up and down for several times, and combined them with the cells in the 15 ml tube. The cell solution was filtered the cells with a 70 μM cell strainer, centrifuged at 1000rpm for 4 min, and resuspended in KSFM medium (Invitrogen, 37010022) supplemented with 0.05 mM CaCl2 (Sigma, C7902), 0.05 μg/ml Hydrocortisone (Sigma, H0888), 5 ng/ml EGF (Invitrogen, 10450-013), 7.5 μg/ml Bovine Pituitary Extract (Invitrogen, 13028-014), 0.5 μg/ml insulin (Sigma, I9278), 100 U/mL penicillin, 100 μg/mL streptomycin, and 25 μg/mL of Amphotericin B (Gibco, 15240062). The cells were gently washed for once in media and seeded in 10 cm dishes with complete KSFM medium. The dishes were pre-coated with collagen (Advanced Biomatrix, 5005-B). keratinocytes from each mouse were seeded in one 10 cm dish and changed into fresh complete KSFM medium after 24 hours. After ~3 to 4 days, the primary keratinocytes to reach 80% confluence under normal culture conditions in 5% CO2, 37°C incubator. For hypoxia experiment, cells were cultured in a sealed chamber with pre-formulated gas mixture (1% O2, 5% CO2, and 94% N2). For keratinocyte differentiation, cells were either left confluent for 2 or 4 days (C2 or C4), or treated with 1 mM CaCl2 for 2 days. Undifferentiated cells were harvested before confluent (Pre-C). For treatment of the cells, H2O2 (Sigma, H1009), UVB irradiation, glutathione (GSH, Sigma, G6013), N-acetyl-Cysteine (NAC, Sigma, A7250), different concentrations of galactose/fructose (Sigma, G5388, F3510), or other substrates were supplemented to the KSFM complete cell culture medium as indicated. Human psoriatic skin equivalents (MatTek, SOR-300-FT) were cultured according to the manufacturers' recommendation and treated topically with WZB117 (25μL; 6 or 30mg/ml in acetone) for 24 hours. The epidermal portions or the skin organoids were isolated and processed for RT-PCR.

In vitro Wound-healing Assay

For the wound-healing assay, cells were plated at a several densities ranging from 0.5–1×106 cells/well in a 6-well plate (3 wells per cell line) and cultured for 24 hours under standard culture conditions. The day of the assay, control and knockout cells showing comparable densities were selected for assessment. Three parallel lines per well were 'drawn' with

gentle pressure, using a sterile 1000 μl pipette tip. Cells were washed twice with PBS to remove cell debris before adding pre-warmed standard culture medium. The plate was then placed into the temperature- and CO2-controlled environmental chamber (OKO lab) of a Nikon Ti Eclipse microscope with perfect focus, motorized stage and Zyla 4.2 sCMOS camera (Andor) driven by a NIS Elements V4.13 software package. Wound closure (1 region of interest per scratch) was recorded by phase contrast using a 10× air objective at a frame rate of 1 image/10 minute for 24 hours. For quantification in ImageJ, the wound area was measured manually in the first and last frame of each dataset (8 per cell line) and results were expressed as efficiency of wound closure (100−[(100/area first frame)*area last frame]).

3H-2-deoxyglucose (2-DG) Uptake Assay

2-DG uptake assays were performed as previously described[49]. Primary mouse or human keratinocytes were seeded in triplicate in 12-well plates overnight (50000), washed twice with PBS (Sigma, D8537), incubated in basic KSFM (without any supplementation) or serum free DMEM/F12 medium (Thermo, 11320033, for SCCT8 cells) for 2 hours, washed twice with KRHP buffer, and incubated in 0.45 ml KRHP buffer to each well, and starved for 30 minutes. For inhibition of glucose transporter, Cytochalasin B (10 μM, Sigma, C6762) and phloretin (100 μM, Sigma, P7912) were added to the KRHP medium for another 15 minutes. Uptake was initiated by adding 1μCi 3H 2-DG (25–30 Ci/mmol, PerkinElmer, NET549) and 0.1 mM unlabeled 2-DG (Sigma, D8375) in KRHP to each well for 10 or 20 min. Transport activity was terminated by the rapid removal of the uptake medium and washing 3 times with cold PBS with 25 mM glucose (Sigma, G7528). Cells were lysed with 0.5 ml of 0.5 M NaOH (Fisher Scientific, SS255-1) and neutralized with 0.5 ml or 0.5 M HCl (Sigma, 320331), mixed well. 250 μl of the lysate was transferred to a scintillation vial with scintillation solution, and the sample was quantitated by liquid scintillation counting. Protein concentrations were determined by BCA assay (Thermo, 23227).

Histological Analyses and Immunoblotting

For immunohistochemistry (IHC), tissues were fixed in 4% paraformaldehyde and embedded in paraffin. Sections (5 μm) were deparaffinized, heat retrieved (buffer with 10 mM Tris, 1.0 mM EDTA, PH=8.0, 94–96 °C for 30min, cool naturally), perforated (0.2% Triton × 100, 10 min), blocked in 3% BSA (Sigma, A9418) and then incubated with Glut1 (1:500, Thermo, RB-9052-P0), K10 (1:500, Santa Cruz, SC-70907), K14 (1:500, Santa Cruz, SC-53253), Loricrin (1:1000, BioLegend, 905104), p-ACC Ser79 (1:400, CST, 3661), p-S6 Ser240/244 (1:2000, CST, 5364), Ki-67 (1:400, Abcam, ab16667), CD45 (1:100, BioLegend 147701), F4/80 (1:50, BioLegend 122602), CD11c (1:100, BioLegend 117301), Gr-1 (1:20, BD Biosciences 550291), and CD4 (1:600, Thermo, 4SM95) primary antibodies. IHC and Hematoxylin (Vector, H3401) and Eosin Y (Thermo, 6766007) staining (HE staining) were performed using standard protocols or under the manufacturer's instructions. Detection of IHC signal was performed with Vectastain Elite ABC kit (Vector Laboratories, Burlingame, CA) and DAB substrate kit for peroxidase (Vector Laboratories) followed by hematoxylin counterstaining (Vector Laboratories). For scoring of leukocytes, four sections from at least three mice per group from at least 2 independent experiments were stained, and photomicrographs were taken of representative 40× magnification fields. Positive cells per

photomicrograph were quantified. For immunofluorescence of Glut1 and K14, after incubation with primary antibody, slides were washed and incubated with Alex Fluor 546 goat-anti-rabbit or Alex Fluor 488 goat-anti-mouse secondary antibody (Life Technology, A11001, A11010) at room temperature for 1 hour, then washed and sealed with ProLong Gold antifade reagent with DAPI (Life technology, P36935). TUNEL staining (ThermoFisher, C10617) was performed according to the manufacturer's protocol. For all histological analyses, the rater, typically a dermatopathologist, was blinded to the genotype and/or treatment condition. For Western blotting, samples of cells or tissues were separated on SDS-PAGE gels, transferred to PVDF membranes and probed with primary antibodies as follows: Glut1 (1:2000, Thermo, RB-9052-P0), K10 (1:500, Santa Cruz, SC-70907), K14 (1:1000, Santa Cruz, SC-53253), HSP90 (1:1000, CST, 4877), Involucrin (1:1000, Thermo, MA5-11803), p-ACC Ser79 and ACC (1:1000, CST, 3661, 3662), p-S6 Ser240/244 (1:4000, CST, 5364), COX IV (1:2000, CST, 4844), and followed by secondary antibodies conjugated to HRP at a dilution of 1:5000 (Santa Cruz, Donkey anti-Rabbit: SC2077, Donkey anti-mouse: SC2096) and detection by the ECL System (PerkinElmer, NEL104001EA). Protein content was quantitated by the BCA protein assay kit (Thermo Pierce, 23227).

RNA extraction and qRT-PCR

Cells or tissues were lysed in Trizol reagents (Sigma, T9424), and mRNA was extracted following the standard protocols, and reversed transcribed using the Thermoscript RT system (Invitrogen, 11146-016) according to the manufacture's instructions. qRT-PCR was performed using Real-Time System (Sybr-green, Applied Biosystems, A25741). Data were normalized to the internal control and presented as a relative expression level. All primers for qRT-PCR are described in Table S1.

Cytometry and Proliferation Measurements

For basal levels oxidative stress, cells were stained with 5 μM DCFDA (Thermo, D-399) for 30 min, cells were washed, trypsinized, collected on ice, centrifuged at 1500 rpm 4min, washed once with FACS buffer (DPBS with 2% FBS (Sigma, F2442) and 0.2 mM EDTA (Ambion, AM9260G)), and then resuspended in FACS buffer for analysis (FACScalibur, BD). For oxidative stress induced by H2O2, cells were supplemented with 5 μM DCFDA, then incubated in the indicated amount of H2O2, and harvested after 30 min of incubation. For oxidative stress induced by UVB irradiation, cells were incubated with 5 μM DCFDA for 10 minutes, took the medium to new tubes, washed the cells once with PBS, irradiated the cells for indicated doses, put the medium back to the cells, incubated for another 20 min, then harvested the for FACS analysis. For cultured cell proliferation, equal cells numbers were seeded, harvested at indicated times, and then counted in the presence of Trypan blue (Biorad, 145-0013). For staining, cells were stained with 0.25% Crystal Violet (Sigma, C0775) in 6.25% ethanol (Pharmco-AAPER, 111000200) for 30min at room temperature, washed 3 times with ddH2O, dried at room temperature, and photographed. For the MTT assay, cells were incubated with 0.5 mg/ml MTT (Thermo, M6494) for 2 hours, dissolved in DMSO (Sigma D4540), and measured the absorbance at 540 nm. For the keratinocytes proliferation in tissues, the tissues were stained with Ki-67 as described in histological analyses section.

ATP Measurements

Cellular ATP content was measured using the CellTiter-Glo Luminescent Assay Kit (Promega, G7570). Briefly, cells were seeded at least triplicate wells at a density of 10000 cells/well in two 96 well plate, and allowed for attachment overnight. One plate of cells was used for measuring the concentrations of protein by BCA method. Another plate of cells were put at room temperature for 30 min, added 100 μl of lysis buffer with CellTiter-Glo® Substrate, mixed well, and shake on an orbital shaker for 15 min at room temperature. Cellular ATP level was measured using a luminescent plate reader (BioTek). A standard curve of ATP was made to make sure the concentrations of cellular ATP were within the linear range.

Lipid Analyses

Epidermis from WT (n=4) and K14.Glut1 (n=4) mice were harvested for lipid analysis. Sphingolipids levels were quantitated using LC-MS/MS methodology[57]. Briefly, flash frozen epidermis scraps were homogenized in 500 μL of ice cold HPLC water using a sonic dismembrator probe, a 50 μL aliquot was reserved for protein determination. Immediately afterwards the aqueous homogenate was quenched by adding it to 2 mL of organic extraction solvent (isopropanol: ethyl acetate, 15:85; vol:vol) in a borosilicate glass culture tube. The original sample tube was rinsed twice with 500 μL of cold HPLC water and the aqueous emulsions were added to the organic extraction solvent. 20 μL of internal standard solution was added (Avanti Polar Lipids, AL Ceramide/Sphingoid Internal Standard Mixture II diluted 1:10 in ethanol). The mixture was vortexed and sonicated in ultrasonic bath for 10 minutes at 40 °C. Then, the samples were allowed to reach room temperature. Two-phase liquid extraction was performed, the supernatant was transferred to a new tube and the pellet was re-extracted. Supernatants were combined and evaporated under nitrogen. The dried residue was reconstituted in 2 mL of Folch solution, 500 μL was transferred to a new tube and reserved for organic phosphate determination. Both organic fractions were dried under nitrogen and stored at −80°C until analysis. Sphingolipids levels were quantitated using LC-MS/MS methodology using a Nexera X2 UHPLC system coupled to a Shimadzu LCMS-8050 triple quadrupole mass spectrometer operating the Dual Ion Source in Electrospray positive mode. Dried lipid extracts were reconstituted in 200 μL of HPLC solvent (methanol/ formic acid 99:1; vol:vol containing 5 mM ammonium formate) for LC-MS/MS analysis. Lipid separation was achieved on a 2.1 (i.d.) × 150 mm Kinetex C8, 2.6 micron core-shell particle (Phenomenex, Torrance, CA) column. Sphingolipids species were identified based on exact mass and fragmentation patterns, and verified by lipid standards. The concentration of each metabolite was determined according to calibration curves using peak-area ratio of analyte vs. corresponding internal standard. Calibration curves were generated using serial dilutions of each target analyte. Sphingolipid true standards were purchased from Avanti Polar Lipids (Alabaster, Al). For total phosphorous determination, total phosphorous content in the organic extracts was determined as described[58].

Metabolite Profiling

Epidermis was harvested from the dorsal skin from *WT* and *K14.Glut1* mice, each epidermal sample was from one mice. 8 pairs of samples were used for metabolomic

analysis as described[59]. The harvested epidermis was snap frozen and metabolites extracted with 80% ice-cold methanol. Metabolite profiling was performed using a liquid chromatography-mass spectrometry/mass spectrometry (LC-MS/MS). The peak area for each detected metabolite was normalized against the total ion count (TIC). The pre-processed datasets were mean-centered and unit-variance scaled. Principal component analysis (PCA) and hierarchical clustering of metabolites in different samples were analyzed using the MetaboAnalyst 3.0.

Microarray Analyses

Primary keratinocytes derived from WT (n=8) and K14.Glut1 (n=8) mice were harvested. Two plates of cells of the same genotype were pooled into 2 groups for each genotype for microarray analysis. Cells were put into the Trizol solution (Sigma, T9424) for extraction of total RNA according to the manufacturer's instructions. 1 μg RNA were reverse transcribed to double stranded cDNA, then transcribed to biotin-labeled cRNA according to the standard Affymetrix protocol. Following fragmentation, 15 μg cRNA of each sample was hybridized for 16 hours at 45°C on GeneChip Mouse Transcriptome Assay 1.0, and scanned at the UTSW Microarray Core Facility. Array scanning was performed according to the manufacturer's instruction (Affymetrix). Raw data were processed with Affymetrix Expression console software for background correction and normalization.

Data Availability

All data supporting the findings of this study are available from the corresponding author upon request. Microarray data from this study have been deposited in GenBank with the accession codes GSE102955.

Supplementary Material

Refer to Web version on PubMed Central for supplementary material.

Acknowledgments

We thank the Ruth Gordillo for help with lipidomic studies; Chendong Yang, Jessica Sudderth, Lauren Zacharias, and Jorge Galvan Resendiz and the Children’s Research Institute Metabolomics Facility for help with metabolomic studies; Lin-chiang Tseng for help with patient sample collection; and Pedram Gerami for help with psoriasis models. This work was supported by the following grants: NCI R35 CA220449-01 and Welch Foundation (I-1733-06) to R.J.D.; NIAMS K23AR061441 to B.F.C.; NIDDK DK10550 to J.C.R.; NIAMS 1R01AR072655, Burroughs Wellcome Fund CAMS (1010978), and American Cancer Society/Simmons Cancer Center (ACS-IRG-02-196) to R.C.W.

References

1. Vander Heiden MG, Cantley LC, Thompson CB. Understanding the Warburg effect: the metabolic requirements of cell proliferation. Science. 2009; 324:1029–1033. [PubMed: 19460998]
2. Palm W, et al. The Utilization of Extracellular Proteins as Nutrients Is Suppressed by mTORC1. Cell. 2015; 162:259–270. [PubMed: 26144316]
3. Comerford SA, et al. Acetate dependence of tumors. Cell. 2014; 159:1591–1602. [PubMed: 25525877]
4. Hensley CT, et al. Metabolic Heterogeneity in Human Lung Tumors. Cell. 2016; 164:681–694. [PubMed: 26853473]

5. Faubert B, et al. Lactate Metabolism in Human Lung Tumors. Cell. 2017; 171:358–371. e359. [PubMed: 28985563]
6. Hui S, et al. Glucose feeds the TCA cycle via circulating lactate. Nature. 2017; 551:115–118. [PubMed: 29045397]
7. Michalek RD, et al. Cutting edge: distinct glycolytic and lipid oxidative metabolic programs are essential for effector and regulatory CD4+ T cell subsets. J Immunol. 2011; 186:3299–3303. [PubMed: 21317389]
8. Pearce EL, et al. Enhancing CD8 T-cell memory by modulating fatty acid metabolism. Nature. 2009; 460:103–107. [PubMed: 19494812]
9. De Bock K, et al. Role of PFKFB3-driven glycolysis in vessel sprouting. Cell. 2013; 154:651–663. [PubMed: 23911327]
10. Schoors S, et al. Fatty acid carbon is essential for dNTP synthesis in endothelial cells. Nature. 2015; 520:192–197. [PubMed: 25830893]
11. Thorens B, Mueckler M. Glucose transporters in the 21st Century. Am J Physiol Endocrinol Metab. 2010; 298:E141–145. [PubMed: 20009031]
12. Cura AJ, Carruthers A. Role of monosaccharide transport proteins in carbohydrate assimilation, distribution, metabolism, and homeostasis. Comprehensive Physiology. 2012; 2:863–914. [PubMed: 22943001]
13. Gherzi R, et al. "HepG2/erythroid/brain" type glucose transporter (GLUT1) is highly expressed in human epidermis: keratinocyte differentiation affects GLUT1 levels in reconstituted epidermis. J Cell Physiol. 1992; 150:463–474. [PubMed: 1537878]
14. Elson DA, Ryan HE, Snow JW, Johnson R, Arbeit JM. Coordinate up-regulation of hypoxia inducible factor (HIF)-1alpha and HIF-1 target genes during multi-stage epidermal carcinogenesis and wound healing. Cancer Res. 2000; 60:6189–6195. [PubMed: 11085544]
15. Tao J, et al. Expression of GLUT-1 in psoriasis and the relationship between GLUT-1 upregulation induced by hypoxia and proliferation of keratinocyte growth. J Dermatol Sci. 2008; 51:203–207. [PubMed: 18565734]
16. Tochio T, Tanaka H, Nakata S. Glucose transporter member 1 is involved in UVB-induced epidermal hyperplasia by enhancing proliferation in epidermal keratinocytes. Int J Dermatol. 2013; 52:300–308. [PubMed: 23330712]
17. Watt SA, et al. Integrative mRNA profiling comparing cultured primary cells with clinical samples reveals PLK1 and C20orf20 as therapeutic targets in cutaneous squamous cell carcinoma. Oncogene. 2011; 30:4666–4677. [PubMed: 21602893]
18. Young CD, et al. Modulation of glucose transporter 1 (GLUT1) expression levels alters mouse mammary tumor cell growth in vitro and in vivo. PLoS One. 2011; 6:e23205. [PubMed: 21826239]
19. Wellberg EA, et al. The glucose transporter GLUT1 is required for ErbB2-induced mammary tumorigenesis. Breast Cancer Res. 2016; 18:131. [PubMed: 27998284]
20. Macintyre AN, et al. The glucose transporter Glut1 is selectively essential for CD4 T cell activation and effector function. Cell Metab. 2014; 20:61–72. [PubMed: 24930970]
21. Liu Y, et al. A small-molecule inhibitor of glucose transporter 1 downregulates glycolysis, induces cell-cycle arrest, and inhibits cancer cell growth in vitro and in vivo. Mol Cancer Ther. 2012; 11:1672–1682. [PubMed: 22689530]
22. Kuehne A, et al. Acute Activation of Oxidative Pentose Phosphate Pathway as First-Line Response to Oxidative Stress in Human Skin Cells. Mol Cell. 2015; 59:359–371. [PubMed: 26190262]
23. Zhang ZZ, et al. Glutathione Depletion, Pentose Phosphate Pathway Activation, and Hemolysis in Erythrocytes Protecting Cancer Cells from Vitamin C-induced Oxidative Stress. J Biol Chem. 2016; 291:22861–22867. [PubMed: 27660392]
24. Schafer M, Werner S. Nrf2--A regulator of keratinocyte redox signaling. Free Radic Biol Med. 2015; 88:243–252. [PubMed: 25912479]
25. Amen N, et al. Differentiation of epidermal keratinocytes is dependent on glucosylceramide:ceramide processing. Human molecular genetics. 2013; 22:4164–4179. [PubMed: 23748427]

26. Jennemann R, et al. Integrity and barrier function of the epidermis critically depend on glucosylceramide synthesis. J Biol Chem. 2007; 282:3083–3094. [PubMed: 17145749]
27. Takashima A, Bergstresser PR. Impact of UVB radiation on the epidermal cytokine network. Photochem Photobiol. 1996; 63:397–400. [PubMed: 8934748]
28. Raja, Sivamani K, Garcia MS, Isseroff RR. Wound re-epithelialization: modulating keratinocyte migration in wound healing. Front Biosci. 2007; 12:2849–2868. [PubMed: 17485264]
29. Hawkes JE, Gudjonsson JE, Ward NL. The Snowballing Literature on Imiquimod-Induced Skin Inflammation in Mice: A Critical Appraisal. J Invest Dermatol. 2016
30. van der Fits L, et al. Imiquimod-induced psoriasis-like skin inflammation in mice is mediated via the IL-23/IL-17 axis. J Immunol. 2009; 182:5836–5845. [PubMed: 19380832]
31. Chan JR, et al. IL-23 stimulates epidermal hyperplasia via TNF and IL-20R2-dependent mechanisms with implications for psoriasis pathogenesis. J Exp Med. 2006; 203:2577–2587. [PubMed: 17074928]
32. Flutter B, Nestle FO. TLRs to cytokines: mechanistic insights from the imiquimod mouse model of psoriasis. Eur J Immunol. 2013; 43:3138–3146. [PubMed: 24254490]
33. Tortola L, et al. Psoriasiform dermatitis is driven by IL-36-mediated DC-keratinocyte crosstalk. J Clin Invest. 2012; 122:3965–3976. [PubMed: 23064362]
34. Van Belle AB, et al. IL-22 is required for imiquimod-induced psoriasiform skin inflammation in mice. J Immunol. 2012; 188:462–469. [PubMed: 22131335]
35. Sa SM, et al. The effects of IL-20 subfamily cytokines on reconstituted human epidermis suggest potential roles in cutaneous innate defense and pathogenic adaptive immunity in psoriasis. J Immunol. 2007; 178:2229–2240. [PubMed: 17277128]
36. Fuchs E. Scratching the surface of skin development. Nature. 2007; 445:834–842. [PubMed: 17314969]
37. Freinkel RK. Metabolism of glucose-C-14 by human skin in vitro. J Invest Dermatol. 1960; 34:37–42. [PubMed: 13824821]
38. Sparks JW, Avery GB, Fletcher AB, Simmons MA, Glinsmann WH. Parenteral galactose therapy in the glucose-intolerant premature infant. J Pediatr. 1982; 100:255–259. [PubMed: 7035638]
39. Barone S, et al. Slc2a5 (Glut5) is essential for the absorption of fructose in the intestine and generation of fructose-induced hypertension. J Biol Chem. 2009; 284:5056–5066. [PubMed: 19091748]
40. Zhao FQ, Keating AF. Functional properties and genomics of glucose transporters. Curr Genomics. 2007; 8:113–128. [PubMed: 18660845]
41. Holden HM, Rayment I, Thoden JB. Structure and function of enzymes of the Leloir pathway for galactose metabolism. J Biol Chem. 2003; 278:43885–43888. [PubMed: 12923184]
42. Cantor JR, et al. Physiologic Medium Rewires Cellular Metabolism and Reveals Uric Acid as an Endogenous Inhibitor of UMP Synthase. Cell. 2017; 169:258–272. e217. [PubMed: 28388410]
43. Hamanaka RB, et al. Mitochondrial reactive oxygen species promote epidermal differentiation and hair follicle development. Sci Signal. 2013; 6:ra8. [PubMed: 23386745]
44. Farber S, Diamond LK. Temporary remissions in acute leukemia in children produced by folic acid antagonist, 4-aminopteroyl-glutamic acid. N Engl J Med. 1948; 238:787–793. [PubMed: 18860765]
45. Heidelberger C, et al. Fluorinated pyrimidines, a new class of tumour-inhibitory compounds. Nature. 1957; 179:663–666. [PubMed: 13418758]
46. Eugui EM, Almquist SJ, Muller CD, Allison AC. Lymphocyte-selective cytostatic and immunosuppressive effects of mycophenolic acid in vitro: role of deoxyguanosine nucleotide depletion. Scand J Immunol. 1991; 33:161–173. [PubMed: 1826793]
47. Greb JE, et al. Psoriasis. Nat Rev Dis Primers. 2016; 2:16082. [PubMed: 27883001]
48. Mehta NN, et al. Systemic and vascular inflammation in patients with moderate to severe psoriasis as measured by [18F]-fluorodeoxyglucose positron emission tomography-computed tomography (FDG-PET/CT): a pilot study. Arch Dermatol. 2011; 147:1031–1039. [PubMed: 21576552]

49. Kamleh MA, et al. LC-MS metabolomics of psoriasis patients reveals disease severity-dependent increases in circulating amino acids that are ameliorated by anti-TNFalpha treatment. J Proteome Res. 2015; 14:557–566. [PubMed: 25361234]
50. Kang H, et al. Exploration of candidate biomarkers for human psoriasis based on gas chromatography-mass spectrometry serum metabolomics. Br J Dermatol. 2016
51. Checa A, et al. Circulating levels of sphingosine-1-phosphate are elevated in severe, but not mild psoriasis and are unresponsive to anti-TNF-alpha treatment. Sci Rep. 2015; 5:12017. [PubMed: 26174087]
52. Lee EE, et al. A Protein Kinase C Phosphorylation Motif in GLUT1 Affects Glucose Transport and is Mutated in GLUT1 Deficiency Syndrome. Mol Cell. 2015; 58:845–853. [PubMed: 25982116]
53. Telang S, et al. Small molecule inhibition of 6-phosphofructo-2-kinase suppresses t cell activation. J Transl Med. 2012; 10:95. [PubMed: 22591674]
54. Koo SW, Hirakawa S, Fujii S, Kawasumi M, Nghiem P. Protection from photodamage by topical application of caffeine after ultraviolet irradiation. Br J Dermatol. 2007; 156:957–964. [PubMed: 17388926]
55. Wang X, Ge J, Tredget EE, Wu Y. The mouse excisional wound splinting model, including applications for stem cell transplantation. Nat Protoc. 2013; 8:302–309. [PubMed: 23329003]
56. Lichti U, Anders J, Yuspa SH. Isolation and short-term culture of primary keratinocytes, hair follicle populations and dermal cells from newborn mice and keratinocytes from adult mice for in vitro analysis and for grafting to immunodeficient mice. Nat Protoc. 2008; 3:799–810. [PubMed: 18451788]
57. Holland WL, et al. An FGF21-adiponectin-ceramide axis controls energy expenditure and insulin action in mice. Cell Metab. 2013; 17:790–797. [PubMed: 23663742]
58. Carles J. Colorimetric microdetermination of phosphorus. Bull Soc Chim Biol (Paris). 1956; 38:255–257. [PubMed: 13329652]
59. Mullen AR, et al. Oxidation of alpha-ketoglutarate is required for reductive carboxylation in cancer cells with mitochondrial defects. Cell Rep. 2014; 7:1679–1690. [PubMed: 24857658]

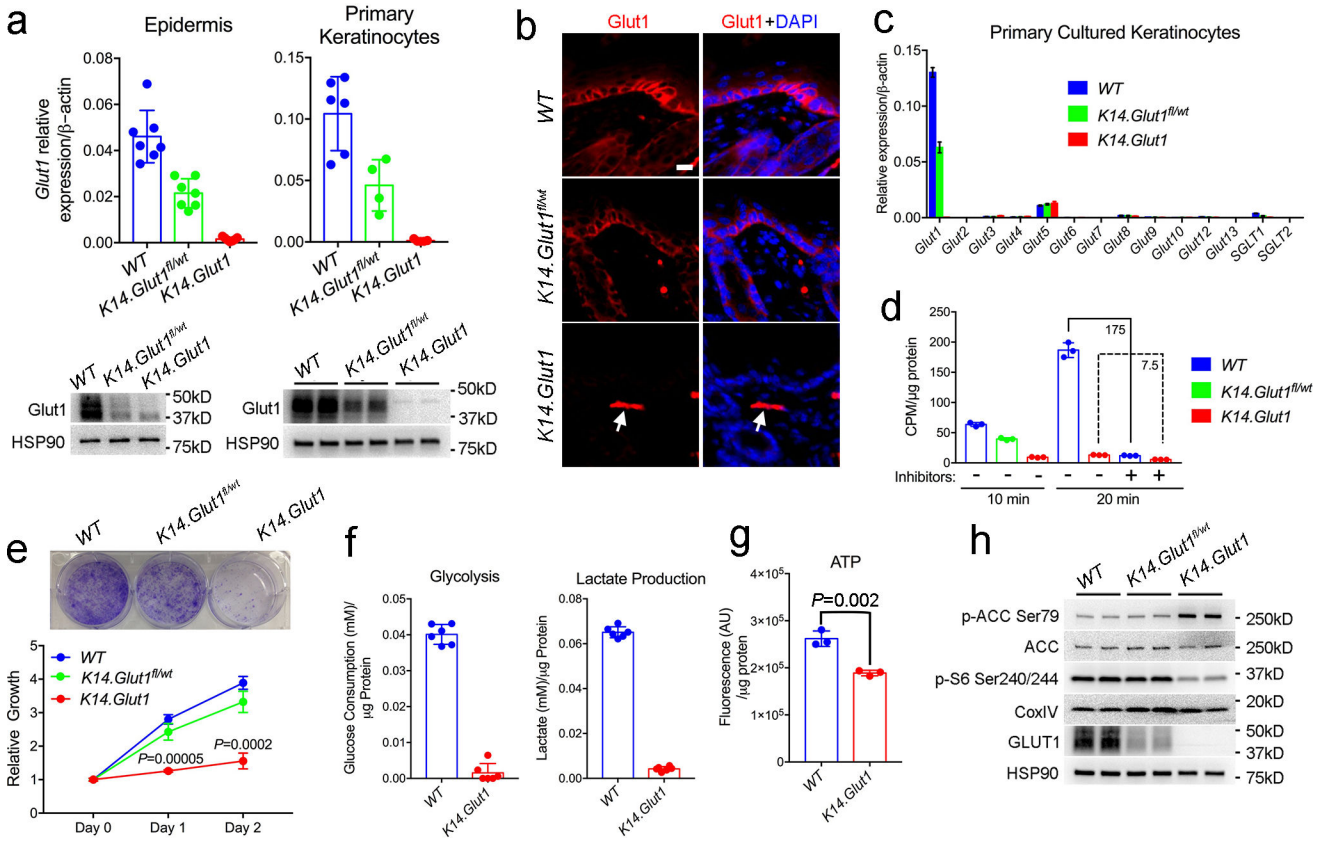

Figure 1. Primary Keratinocytes Showed Impaired Proliferation upon *Glut1* Deletion

(a) *Glut1* mRNA (n=4 mice per genotype) and protein levels in the epidermis and primary keratinocytes harvested from one week old *WT, K14.Glut1*$^{fl/wt}$, and *K14.Glut1* mice. **(b)** Immunostaining of Glut1 in skins from one-week old mice. Glut1 staining is absent in epidermis from *K14.Glut1* mice. Arrow indicates persistence of Glut1 staining in the dermis (e.g. dermal endothelial cell). Similar results obtained in 3 independent experiments. **(c)** mRNA abundance of *Glut/SGLT* family members in primary cultured *WT, Glut1*$^{fl/wt\ K14Cre}$, and keratinocytes from *K14.Glut1* mice (n=4 mice per genotype). **(d)** 2-Deoxy-D-glucose uptake in primary cultured keratinocytes obtained from one week old *WT, K14.Glut1*$^{fl/wt}$, and *K14.Glut1* mice with or without glucose inhibitor pretreatment. Similar results obtained in uptake assays from keratinocytes from 3 independent mice. **(e)** Growth rate as assessed by Crystal Violet staining and relative cell number in primary *WT, K14.Glut1*$^{fl/wt}$, and keratinocytes from *K14.Glut1* mice. Identical numbers of cells were seeded in triplicate wells in 6 well plates at day 0. For Crystal Violet staining, cells were stained 3 days after seeding and similar results were obtained in 3 keratinocytes preparations. Keratinocytes from *K14.Glut1* mice show significantly decreased growth compared to keratinoctyes from *WT* controls at day 1 and 2 after plating. **(f)** Glucose consumption and lactate production over 12 hours as measured from the media of primary cultured *WT* and *K14.Glut1* (n=3 mice per genoptye) keratinocytes. **(g)** ATP levels (luminescence) were determined in primary keratinocytes from *WT* and *K14.Glut1* (n=3 mice per genotype) and normalized to protein levels. **(h)** Western Blot analysis of the expression of p-ACC Ser79, ACC, p-S6 Ser240/244, Glut1 in primary keratinocytes obtained from *WT, Glut1*$^{fl/wt\ K14Cre}$ and

K14.Glut1 mice. Data shown as mean±s.d. *P* values were calculated by two-tailed *t*-test. Results were confirmed in at least 2 independent experiments.

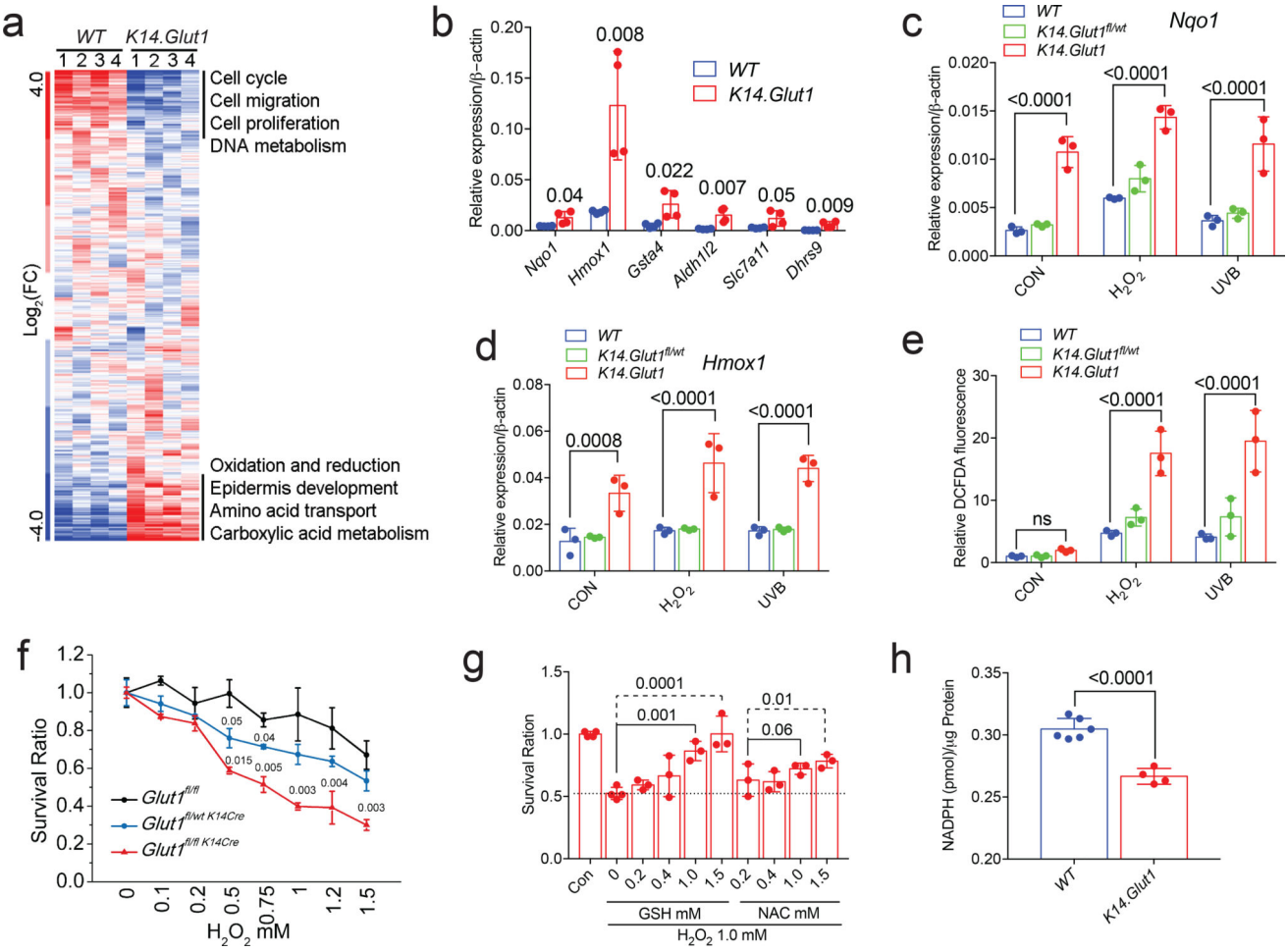

Figure 2. Glut1 Is Required for Proliferation and Redox Homeostasis in Primary Keratinocytes

(a) Hierarchical clustering of transcriptional profiles from keratinocytes from *WT* and *K14.Glut1* mice. Labels identify gene clusters showing enrichment gene ontology analyses (n=8 mice per genotype). **(b)** RT-PCR measurement shows significant upregulation of the indicated redox genes in keratinocytes from *K14.Glut1* and *WT* mice (n=4 mice per genotype). **(c–d)** *Nqo1* and *Hmox1* mRNA abundance in indicated with and without H_2O_2 (100μM) or UVB (10mj/cm^2) stimulation for 6 hours (n=3 mice per genotype). **(e)** FACS analysis of the fluorescence after DCFDA staining of the indicated keratinocytes with and without H_2O_2 (100μM, 30min) and UVB (10mj/cm^2, 30min) stimulation (n=3 independent mice per genotype). **(f)** Keratinocytes were incubated with different concentrations of H_2O_2 for 24 hours. Survival is plotted as a ratio of number of surviving cells compared to the number of plated cells per genotype without H_2O_2 treatment (n=3 mice per group). **(g)** Keratinocytes were pre-treated with Glutathione (GSH) or N-acetyl-cysteine (NAC), and then incubated with H_2O_2 for 24 hours. Survival is plotted relative to untreated controls. **(h)** Keratinocytes from *K14.Glut1* mice show significantly lower levels of NADPH (n=4 mice per genoptype). Data are shown as mean±s.d. *P* values (indicated about relevant comparison) were calculated by two-tailed *t*-test (b, h), two-way ANOVA with Tukey's tests (c–e), and

one-way ANOVA with Dunnett tests (g). Results were confirmed in at least 2 independent experiments.

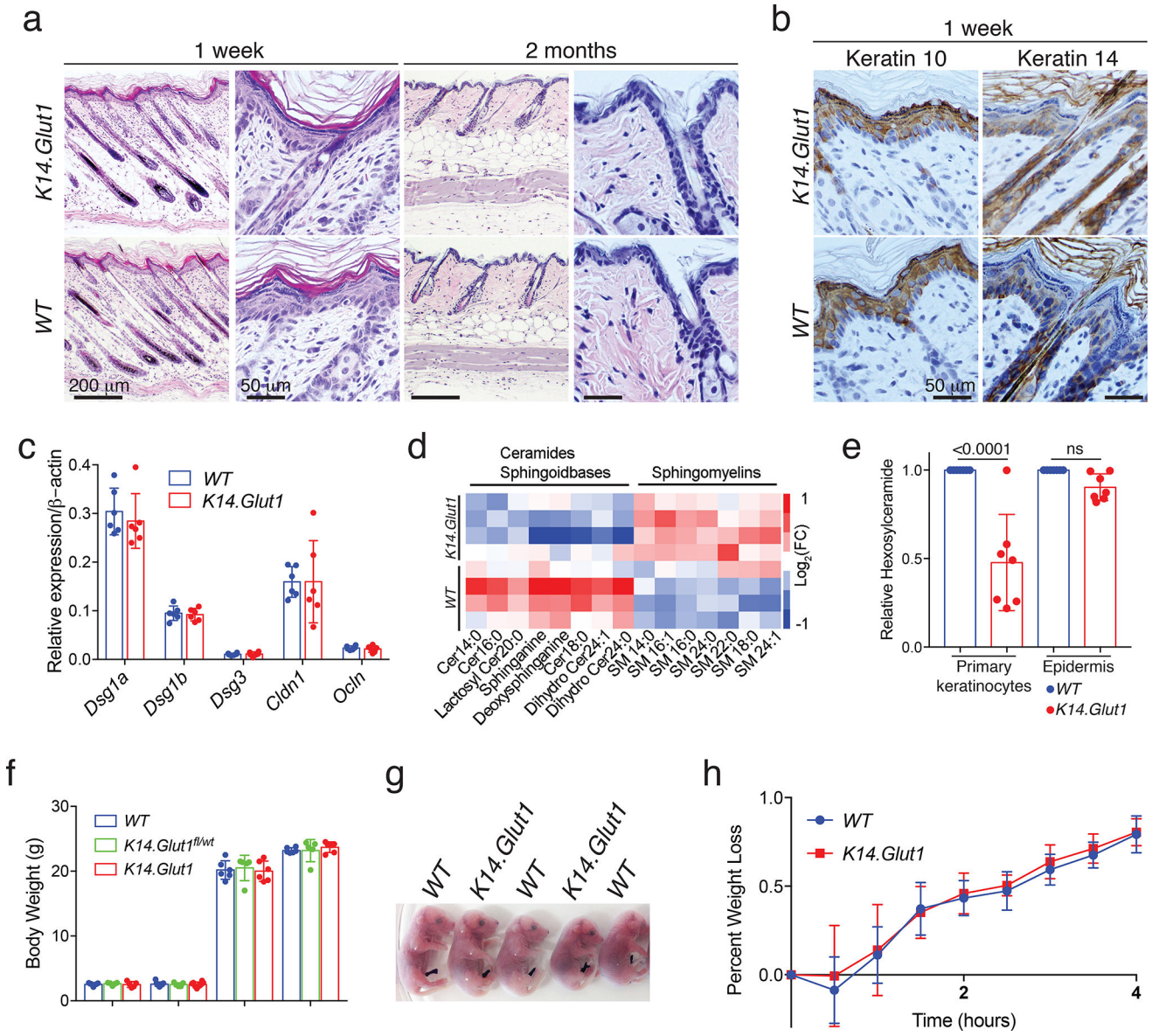

Figure 3. Glut1 is Dispensable for Normal Epidermal Development and Differentiation and its Deletion Induces Metabolic Reprogramming

(a) Histologic section (H&E stained) of skin from one week- and 2 month- old *WT, Glut1*$^{fl/wt\ K14Cre}$ and *K14.Glut1* mice show no histologic differences between the mice. Similar results obtained in 4 independent experiments. **(b)** Immunohistochemistry for Keratin 10 (K10) and K14 show no differences in the respective suprabasal and basal expression for the epidermal keratins. **(c)** RT-PCR measurement of keratinocyte adhesion genes—*Dsg1a* (*Desmoglein 1a*), *Dsg1b, Dsg3, Cldn1* (*Claudin 1*), *Ocln* (*Occludin*)—in the epidermis show no differences between *K14.Glut1* and *WT* epidermis (n=4 mice per genotype). **(d)** Epidermal lipids were isolated from flash frozen epidermis and analyzed by LC-MS/MS. Heat map representation of epidermal lipids demonstrates decreased free ceramides and increased sphingomyelins in the skin of *K14.Glut1* mice (n=4 mice per genotype). **(e)** In vitro keratinocytes, but not epidermis, from *K14.Glut1* mice, showed

significantly decreased levels of hexosylceramides. Each point represents a distinct hexosylceramide species (n=4 mice per genotype). **(f)** Body weights of the 5-day-old and 2-month-old female and male mice of the indicated genotype, showed no significant differences between littermates (n=5 mice per genotype). **(g)** Toluidine Blue staining of E18.5 embryos indicated no differences in epidermal permeability between *WT* and *K14.Glut1* mice. Similar results obtained in 3 independent stainings. **(h)** Neonatal *WT* (n=8 mice) and *K14.Glut1* (n=5 mice) littermates showed no differences in weight loss suggesting no differences transepidermal water loss was intact. Data are shown as mean±s.d. *P* values were calculated by one-way ANOVA with Sidak correction (e). Results were confirmed in at least 2 independent experiments.

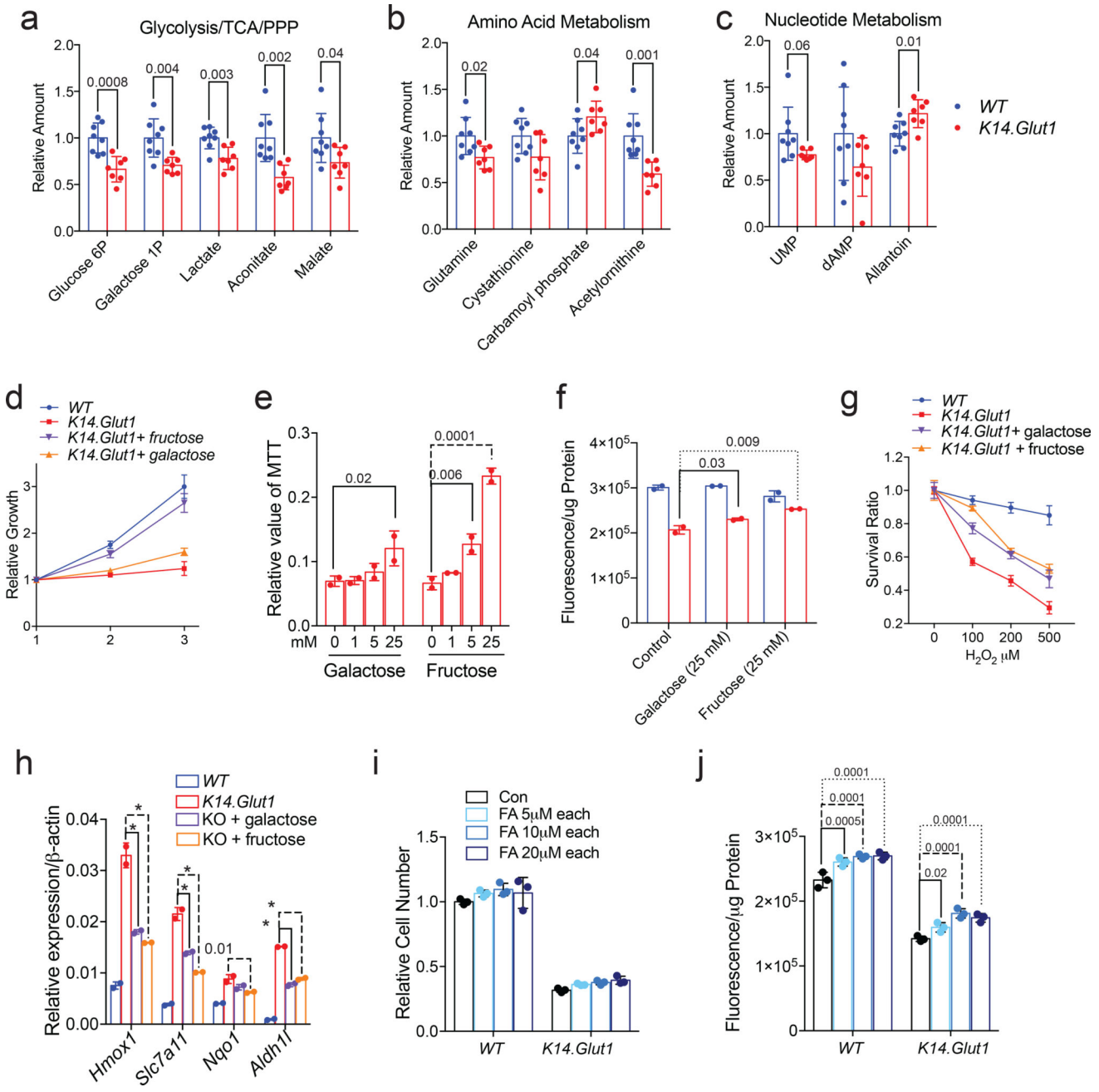

Figure 4. Alternative Hexoses and Fatty Acids Can Partially Rescue Glut1 Deficiency in Keratinocytes

(a–c) Metabolites were extracted from the epidermis of *WT* and *K14.Glut1* mice and analyzed by LC-MS/MS (n=8 mice per genotype). The labeled metabolites represent a subset of metabolites showing significant changes in the (a) glycolysis/TCA/PPP, (b) amino acid metabolism/urea cycle, and (c) nucleotide metabolism. **(d)** Primary keratinocytes from *K14.Glut1* mice were supplemented with galactose (25 mM) or fructose (25 mM) and cell proliferation was assessed by the MTT assay. Similar results obtained in 3 independent experiments. **(e)** Different concentrations of the indicated hexose were supplemented to keratinocytes from *K14.Glut1* mice and cell proliferation was assessed by MTT assay after

36 hours (n=2 mice per genotype). **(f)** ATP concentration in keratinocytes from *K14.Glut1* and *WT* mice was measured with and without hexose supplementation for 36 hours (n=2 mice per genotype). **(g)** Keratinocytes from *K14.Glut1* and *WT* mice were incubated with different concentrations of H_2O_2 for 24 hours with or without hexose supplementation. Survival is calculated relative to the non-H_2O_2 treated cells of each group. Similar results in 3 independent experiments. **(h)** Redox genes expression was measured in keratinocytes from *K14.Glut1 and WT* mice supplemented with hexose supplementation for 36 hours (n=2 mice per genotype). **(i)** Keratinocytes from *K14.Glut1 and WT* were supplemented with different concentrations of fatty acids (1:1 palmitate:oleate, FA) for 36 hours, cell number **(j)** and ATP production **(k)** were assessed. ATP production was normalized by protein levels (n=3 mice per genotype). Data are shown as mean±s.d. *P* values (indicated above relevant comparison) were calculated by two-tailed *t*-test (a–c), two-way ANOVA with Dunnett tests (e, f, h, j). Results were confirmed in at least 2 independent experiments.

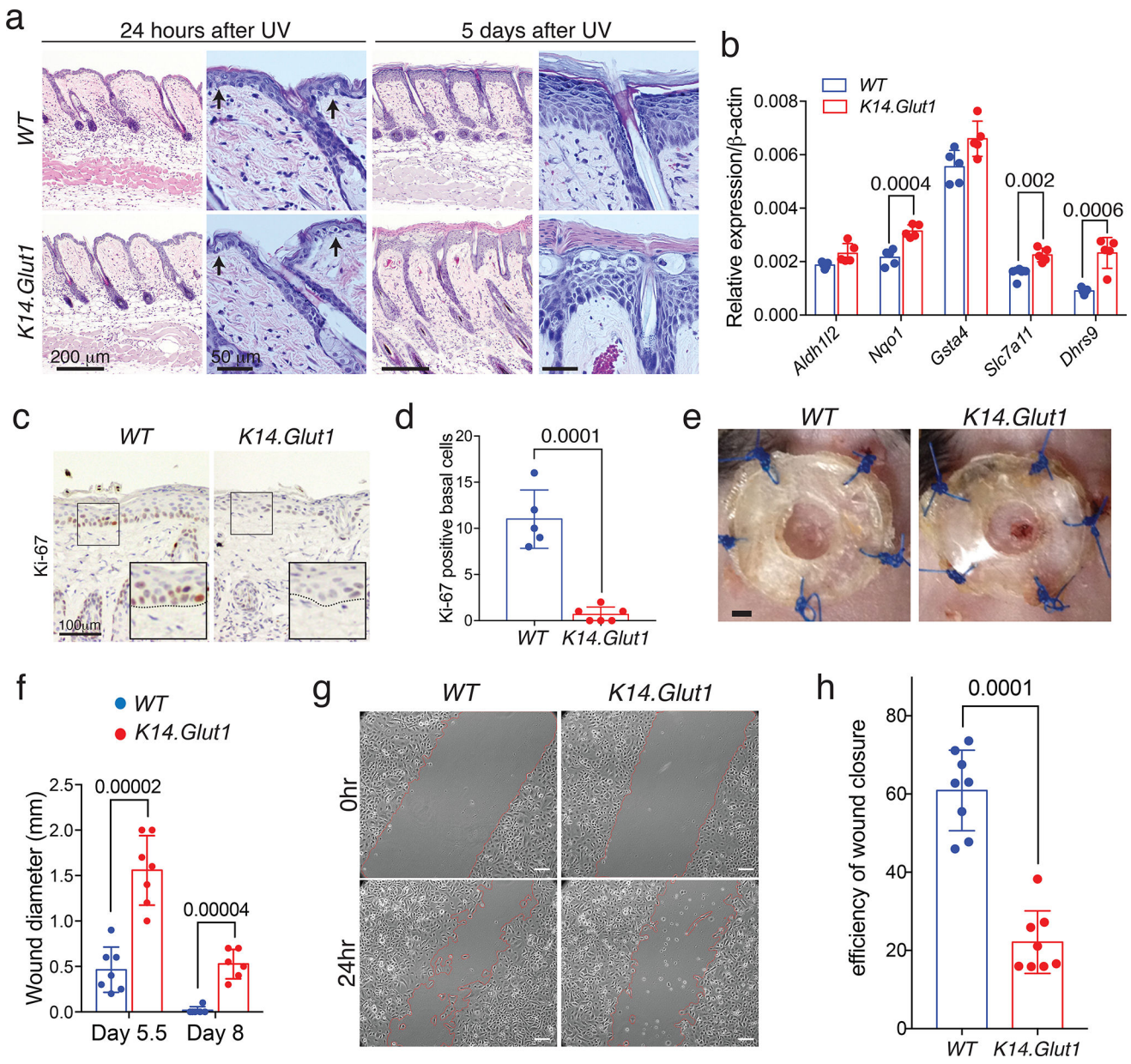

Figure 5. Glut1 Is Required for Proliferation in Response to UVB Irradiation and Wounding

(a) Histologic analyses of UVB (50mj/cm^2) irradiated skin from *WT* and *K14.Glut1* mice. Skin was harvested for analysis at 24 hours and 5 days after UVB. Arrows highlight the presence of apoptotic keratinocytes in both the skin of *WT* and *K14.Glut1* mice. Similar results obtained in 5 independent experiments. **(b)** RT-PCR for redox homeostasis genes from the epidermis of one week old *WT* and *K14.Glut1* (n=5 mice per genotype) mice 6 hours after 50mj/cm^2 UVB irradiation. **(c)** Cell proliferation as assessed by Ki-67 immunostaining 3 days after UVB irradiation. Similar results obtained in 3 independent experiments. **(d)** Significantly fewer Ki-67 basal keratinocytes were identified in *K14.Glut1* mouse skin (n=3 mice per genotype). **(e)** Photo of splinted excisional wounds on the dorsal back revealed that *K14.Glut1* mice had not completely healed wounds compared to their

wildtype littermates after 8 days. Similar results obtained in 7 independent experiments. **(f)** Wound diameters in *WT* and *K14.Glut1* mice (n=7 mice per genotype) 5.5 and 8 days after wounding. **(g)** Live cell imaging reveals that keratinocytes from *K14.Glut1* mice show defects in closure of a scratch assay *in vitro*. Red lines indicate keratinocytes that have migrated from the wound edge. Scale bar, 50 μm. Similar results obtained in 3 independent experiments. **(h)** Quantitation of wound closure as a percentage of the initial wound reveals that keratinocytes from *K14.Glut1* mice are significantly impaired in their ability to migrate and close wounds in vitro. (n=3 mice per genotype). Data are presented as mean±s.d.; *P* values (indicated above relevant comparison) were calculated by two-tailed *t*-test. Results were confirmed in at least 2 independent experiments.

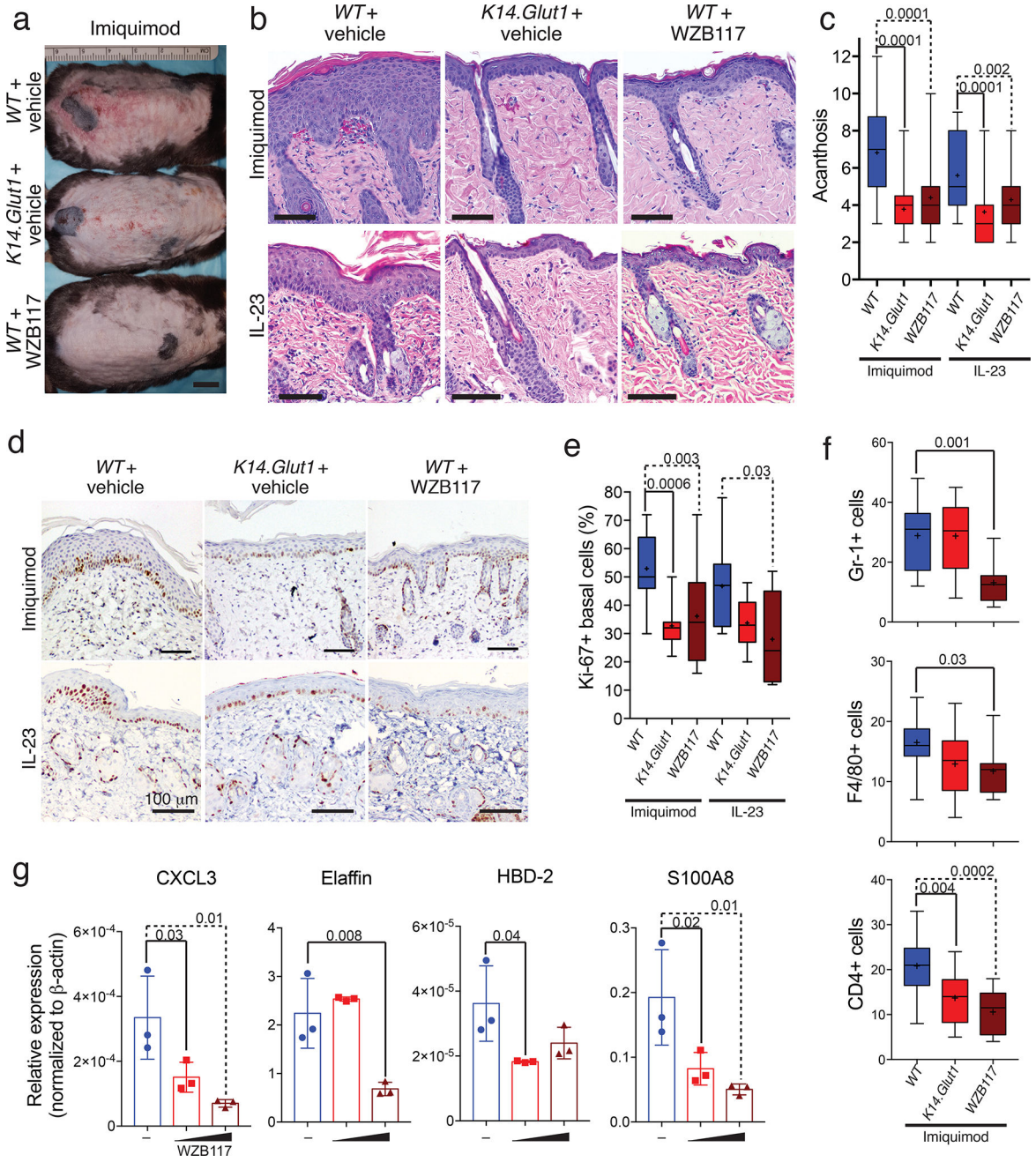

Figure 6. Genetic or Topical Inhibition of Glucose Transport Decreases Psoriasiform Hyperplasia

(a) *K14.Glut1* have less scale and erythema compared to *WT* littermates after treatment with imiquimod. Similar results obtained in 3 independent experiments. Bar=1cm **(b)** Histologic sections that both genetic (*K14.Glut1*) or chemical (WZB117) inhibition of glucose transport decrease the acanthosis and parakeratosis induced by both imiquimod or IL-23 injections. Similar results obtained in 4 independent experiments. Bar=100 μm. **(c)** *K14.Glut1* and WZB117 treated skin showed significantly less acanthosis after both imiquimod or IL-23 induced psoriasiform dermatitis. Acanthosis was scored blindly as the

number of nucleated keratinocytes (n=6 mice per group). **(d)** Ki-67 staining (5 days) after imiquimod or IL-23 induced psoriasiform dermatitis treatment revealed significantly less proliferation in *K14.Glut1* and WZB117 treated mice. Similar results obtained in 3 independent experiments. **(e)** The percentage of Ki-67 positive cells in epidermal basal cells (per 50 cells) was quantified in skin sections from control, *K14.Glut1*, or and WZB117 (n=6 mice per group). **(f)** *WT, K14.Glut1*, or WZB117 treated mice were treated with imiquimod for 6 days and skin section stained with the specified markers (n=4 mice per group). Treatment with WZB117 significantly decreases the number of leukocytes (CD45+), neutrophils (Gr-1+), macrophages (F4/80+), and T cells (CD4+) induced by imiquimod. **(g)** Human psoriatic skin organoids were treated with vehicle or WZB117 (6 or 30 mg/ml) for 24 hours. The epidermis of the skin organoids were harvested and psoriatic biomarkers analyzed by RT-PCR (n=3). Box shows 25^{th}–75^{th} percentiles, whiskers show min to max, crosses show means, and lines show medians. Bars show mean±s.d.. *P* values (indicated about relevant comparison) were calculated by one-way ANOVA with Holm-Sidak tests (c, e, f, g). Results were confirmed in at least 2 independent experiments.